

Theory for Swap Acceleration near the Glass and Jamming Transitions

Carolina Brito,¹ Edan Lerner,² and Matthieu Wyart³

¹*Instituto de Física, UFRGS, 91501-970, Porto Alegre, Brazil*

²*Institute for Theoretical Physics, University of Amsterdam,
Science Park 904, 1098 XH Amsterdam, The Netherlands*

³*Institute of Physics, EPFL, CH-1015 Lausanne, Switzerland*

(Dated: December 3, 2024)

Swap algorithms can abolish the glass transition, a recent unexplained observation leading to stringent constraints on the nature of this phenomenon. Here we show that swap dynamic is governed by an effective potential describing both particle interactions as well as their ability to change size. Requiring its stability is more demanding than requiring it for the potential energy alone, implying that mechanically stable configurations appear at lower temperatures with swap dynamics. This result leads to a real-space explanation for the speed up swap induces, and allows us to predict key aspects of the structure and elasticity of glass configurations reachable with swap. In particular for continuously poly-disperse systems we predict the jamming transition to be dramatically altered, as we confirm numerically. Our results support that the glass transition is controlled by vibrational properties rather than by thermodynamic ones. A surprising practical outcome of our analysis is a new algorithm that generates ultra-stable glasses by simple descent in an appropriate effective potential.

PACS numbers: 64.70.Pf, 65.20.+w, 77.22.-d

Understanding the mechanisms underlying the slowing down of the dynamics near the glass transition is a long-standing challenge in condensed-matter [1, 2]. Unexpectedly, swap algorithms [3, 4] (in which particles of different radii can swap in addition to the usual moves of particle positions) were recently shown to allow for equilibration of liquids far below the glass transition temperature T_g [5–8]. For judicious choice of poly-dispersity, one finds that: (i) the glass transition near T_g is abolished: with swaps the α -relaxation time is only two or three order of magnitudes slower than in the liquid, instead of 15 orders of magnitude for regular dynamics. (ii) The spatial extent of dynamical correlations, which are significant near T_g , are greatly reduced. (iii) The Debye-waller factor is increased significantly in this temperature range [7]. (iv) The slowing down of the dynamics and the emergence of dynamical correlations do occur, but at a lower temperature, which we refer to as $T_g = 0^{\text{swap}}$. These observations constrain theories of the glass transition. In particular, frameworks in which the slowing-down of the dynamics is controlled by a growing thermodynamic length are ruled out in these materials, as their predictions should be insensitive to the choice of moves set in any Monte-Carlo, as long as these involve a small number of particles [9]. A theory of the glass transition should explain both swap and non-swap dynamics. Goldstein [10] proposed that the glass transition is initiated by a transition in the free energy landscape: at high temperature, the system leaves near saddles, whereas below some temperature T_0 the dynamics can only occur by activation, and is thus much slower. In mean-field models of structural glasses such a transition in the landscape is predicted [11–14] and corresponds to a Mode Coupling Transition (MCT) where the relaxation time diverges. It was suggested that the MCT transi-

tion would be shifted to lower temperature with swap dynamics in [9], as proven and confirmed numerically in a mean-field model of glasses [15]. Yet, understanding the real-space mechanisms underlying the speed up induced by swap in finite dimensions (where the relaxation time cannot diverge) as well as the nature of the very stable glassy configurations swap can reach remains a challenge.

In this Letter we perform a real space analysis of mechanical stability on vibrational time scales under swap dynamics. For traditional (non-swap) dynamics, stability was studied in particular in hard [16–18] and soft spheres [18, 19] systems, where it is controlled by the pressure p and some measure of how particles are connected, the excess coordination $\delta z = z - z_c$ with respect to the isostatic value $z_c = 2d$ where d is the spatial dimension. (In hard spheres, defining the coordination requires averaging on vibrational time scales [16]). A marginal stability line can be computed that separates stable and unstable configurations, as illustrated in Fig.1 for hard spheres. Under a slow compression the system follows a line (in red) in the $(p, \delta z)$ plane. Mechanical stability is reached only for $p > p_0$, the onset pressure where the dynamic becomes activated and vibrational modes become stable, in consistence with Goldstein’s proposal. As p increases past p_0 , relaxation can occur along less and less modes, and the dynamics become more cooperative [9] [40]. In these materials, deeper in the glass phase the system eventually reaches back the stability line, and undergoes a sequence of buckling events that leave it *marginally stable* [17–19]. Marginal stability implies the presence of soft elastic modes (that differs from Goldstone modes) up to nearly zero frequency, and fixes the scaling properties of both structure and vibrations as jamming is approached [18, 19]. These results, valid in finite dimensions, have been quantitatively confirmed in infinite dimension cal-

culations [20–22]. The point where buckling sets in was argued to be a sharp transition, coined Gardner, where the free energy landscape fractures in a hierarchical way [20], as supported by numerical studies in finite dimensions [23]. For very rapid quenches (as those we will perform below) it was argued that the entire glass phase should be marginal [17, 20].

Here we prove that when swap moves are introduced in the dynamics of a poly-disperse system, its vibrational modes are softened. This result explains why the Debye-waller factor is increased in swap dynamics. Most importantly, it implies that the line governing stability in the $(p, \delta z)$ plane is shifted toward larger pressure and coordination, as illustrated by the green line in Fig.1, Right. As a consequence, the onset pressure where the dynamics becomes activated and spatially correlated satisfied $p_0^s > p_0$, explaining observations (i, ii, iv) above. In particular in the range $p_0 < p < p_0^s$, swap dynamic is much faster because it displays collective vibrational modes along which the free energy is essentially flat, while for the traditional dynamics activation above barriers is necessary. For continuous poly-dispersity, we find that these collective modes describe the position of the particles as well as their own size, whose stiffness is inversely proportional to the characteristic width α of the particle size distribution. Beyond our results on the glass transition, our analysis makes stringent predictions on the glass phase and the jamming transition obtained with swaps. We find that isostaticity is lost, e.g. for soft spheres $\delta z \sim \alpha^{1/2} > 0$ as jamming is approached. We predict the scaling of the vibrational spectrum with distance to jamming. All these results are verified numerically by quenching rapidly (so as to explore marginally stable configurations) soft spheres with internal degrees of freedom. Overall, our analysis provides a unifying framework for the glass and the jamming transition that encompasses both swap and non-swap dynamics.

Swap and effective potential: We consider a system of N particles with continuous polydispersity $\rho(R)$, of width $\alpha = \langle (R^2) - \langle R \rangle^2 \rangle^{1/2}$ and whose mean defines our unit length $\langle R \rangle = 1$. Here $\{R\}$ indicates the set of particle radii and $\{r\}$ their positions. We denote by $\mathcal{U}(\{r\}, \{R\})$ the total potential energy in the system. We define the partition function $Z(\{r\})$ annealed over the particle radii:

$$Z(\{r\}) = \sum_{\mathcal{P}(\{R\})} \exp(-\beta \mathcal{U}(\{r\}, \{R\})), \quad (1)$$

where the sum is on all the permutations $\mathcal{P}(\{R\})$ of the particle radii. In the thermodynamic limit, a grand-canonical formulation is equivalent, in which particles of different radii correspond to different species. The associated partition function writes:

$$Z_{GC}(\{r\}) = \sum_{\{R\}} \exp[-\beta(\mathcal{U}(\{r\}, \{R\}) + \sum_i \mu(R_i))], \quad (2)$$

where $\mu(R)$ is the chemical potential at radius R . It is

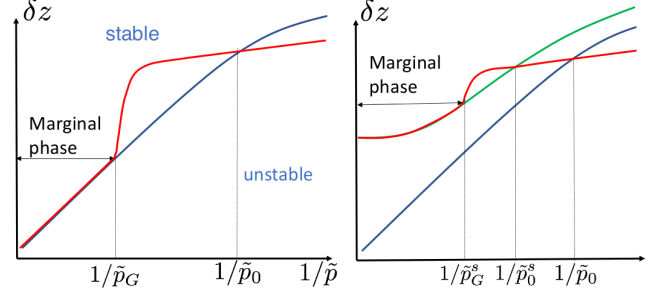


FIG. 1: Log-log representation of the stability diagram in the coordination $\delta z = z - z_c$ and rescaled pressure $\tilde{p} = p/T$ plane for continuously poly-disperse thermal hard spheres with normal (Left) and swap (Right) dynamics. Note that for hard spheres \tilde{p} is independent of temperature and diverges at jamming. In the Left panel, the blue line separates mechanically stable and unstable configurations. The red line indicates the trajectory of a system under a slow compression. When \tilde{p} reaches the onset pressure \tilde{p}_0 , metastable states appear and the dynamic becomes activated and spatially correlated. In the glass phase, the red trajectory will depend on the compression rate, but will eventually reach the blue line at some (rate-dependent) \tilde{p}_G . When this occurs, a buckling or Gardner transition takes place where the material becomes marginally stable, leading to a power-law relation between \tilde{p} and δz . Right: for swap dynamics, stability is more demanding and is achieved only on the green line, which differs strictly from the blue one. Thus the onset pressure increases to some value $\tilde{p}_0^s > \tilde{p}_0$: the dynamics become activated and correlated at larger values of pressures, shifting the position of the glass transition. Marginality is still expected beyond some pressure \tilde{p}_G^s , but leads to plateau value for the coordination, indicating that isostaticity is lost.

chosen such that in the thermodynamic limit, the distribution of radii that follows from Eq. (2) is $\rho(R)$ [41]. A key remark is that once Eq. (2) is integrated on particle position $\{r\}$, one obtains the partition function for the coupled degrees of freedom $\{r\}$ and $\{R\}$ with an effective energy functional:

$$\mathcal{V}(\{r\}, \{R\}) = \mathcal{U}(\{r\}, \{R\}) + \sum_i^N \mu(R_i). \quad (3)$$

Let us consider an athermal system (our arguments can readily be extended to thermal systems such as hard spheres by annealing further the interaction potential on vibrational motion [17, 22, 24]). Mechanical stability under swap dynamics requires \mathcal{V} to be at a minimum. Beyond the usual force balance condition, it implies:

$$\frac{\partial \mathcal{U}}{\partial R_i} \equiv \sum_j f_{ij} = -\frac{\partial \mu}{\partial R} \Big|_{R=R_i^*} \quad (4)$$

where f_{ij} are the contact forces between particle i and j (positive in our notations for repulsive forces), and $(\{r^*\}, \{R^*\})$ the particle positions and radii at the minimum. For unimodal distribution $\rho(R)$, one expects $\mu(R)$ to be

unimodal too. Since in an amorphous solid the fluctuations of the left hand side of Eq. (4) will be of order of the pressure p . To achieve a distribution of radii of width α , the stiffness k_R acting on each particle radius must be of order $k_R \equiv \langle \partial^2 \mu / \partial^2 R \rangle_i \sim p/\alpha$, where the average is made on all particles i .

Generalised vibrational modes: Stability also requires the Hessian H_{swap} (the matrix of second derivatives of \mathcal{V}) to be positive definite. Since they are now $N(d+1)$ degrees of freedom, H_{swap} is a $N(d+1) \times N(d+1)$ symmetric matrix, of eigenvalues ω_{swap}^2 . It contains a block of size $Nd \times Nd$ which is the regular Hessian $H_{ij} = \partial^2 U / \partial r_i \partial r_j$, of eigenvalues ω^2 . It is clear from this block structure that H_{swap} has lower eigenvalues than H [42] (see also below), implying that mechanical stability is more stringent with swap dynamics. Thus the marginal stability line for the swap must be strictly contained in the stable phase of non-swap dynamics, as illustrated in Fig. 1 left.

Let us illustrate this result perturbatively when $k_R \gg k$, where k is the characteristic stiffness of the interaction potential \mathcal{U} , taken as our unit stiffness in what follows. In general, the eigenvalues of H are functions of the set of stiffnesses $\{k_{ij}\}$, but also of the interaction forces $\{f_{ij}\}$ [25]. We first ignore the effects induced by such pre-stress. Moving along a normal mode of H (while leaving the radii fixed) leads to an elastic energy $\sim \omega^2$ and change forces by a characteristic amount δf satisfying $\delta f^2 \sim \omega^2$. Because of such change, Eq. (4) is not satisfied anymore. Thus the potential \mathcal{V} can be reduced further if the radii are allowed to adapt, by an amount of order $\delta f^2/k_R \sim \omega^2/k_R$, and we obtain:

$$\omega^2 - \omega_{\text{swap}}^2 \sim \omega^2/k_R \sim \omega^2 \alpha/p \quad \text{for } p \gg \alpha \quad (5)$$

Jamming transition for soft spheres under swap: We consider soft spheres with half-sided harmonic interactions. In materials with such finite-range interactions, the vibrational spectrum is strongly affected by excess number of constraints δz with respect to the Maxwell threshold where the numbers of degrees of freedom and constraints match. Effective medium [26] or a variational argument [27] imply that in the absence of pre-stress, soft normal modes in the Hessian must be present with eigenvalues $\omega^{*2} \sim \delta z^2$. For swap, Eq. (5) implies that the presence of soft modes at even lower frequencies $\omega_{\text{swap}}^{*2} \sim \delta z^2 (1 - C_0 \alpha/p)$ where C_0 is a numerical constant. Pre-stress can be shown to shift eigenvalues of the Hessian by some amount $\sim -p$ [19, 28], leading to soft modes of frequency ω^0 satisfying $\omega_{\text{swap}}^{02} \sim \delta z^2 (1 - C_0 \alpha/p) - C_1 p$. Mechanical stability requires $\omega_{\text{swap}}^{02} > 0$ and we obtain:

$$\delta z \geq \sqrt{\frac{C_1 p}{1 - C_0 \alpha/p}} \quad \text{for } p \gg \alpha \quad (6)$$

Marginal stability corresponds the equality of Eq. (6), leading to $\delta z \sim \sqrt{p/(1 - C_0 \alpha/p)}$. This is above (but very close to, in the limit $\alpha/p \rightarrow 0$) the bound for non-swap

dynamics of [19], recovered by setting $\alpha/p = 0$. Thus in this limit we expect very small change of structure in the glass phase between swap and non-swap dynamics.

When $p \ll \alpha$, then $k_R \ll 1$: in this regime the stiff constraints correspond to interaction between particles in contact. As far as the low-frequency end of the spectrum is concerned, these interactions can be considered to be hard constraints. The number of degrees of freedom left once these hard constraints are satisfied is $N(d+1) - Nz/2 = N - N\delta z/2$. The number of soft constraints left is simply N , of strength k_R . If δz is small we are thus very close to a Maxwell threshold where the number of degrees of freedom and constraint balance each other, and we can use the same results for the spectrum discussed above. In particular if pre-stress is not accounted for, a plateau of soft modes must appear above some frequency scale:

$$\omega_{\text{swap}}^* \sim \delta z \sqrt{k_R} \sim \sqrt{\frac{p}{\alpha}} \delta z \quad (7)$$

and up to some frequency $\omega_i \sim \sqrt{k_R}$. When pre-stress is accounted for, eigenvalues of the Hessian are again shifted by $\sim -p$. Mechanical stability then implies $p/\alpha \delta z^2 > C_2 p$ and:

$$\delta z \geq C_2 \sqrt{\alpha} \quad \text{for } p \ll \alpha \quad (8)$$

In this regime, marginal stability (the saturation of the stability bound of Eq. 8) corresponds to a coordination independent of pressure, with $\delta z \sim \sqrt{\alpha}$ and $\omega_{\text{swap}}^* \sim \sqrt{p}$. We thus predict that swap dynamics destroys isostaticity, and significantly affect structure and vibrations. For sufficiently large α , this regime will include the entire glass phase. This is the situation sketched in Fig. 1.

Note that these predictions apply to algorithms that allow for swap moves up to the jamming threshold. This is not the case e.g. in [29], where swaps are used to generate dense equilibrated liquids, that are then quenched without swap toward jamming. We also expect isostaticity to be restored in algorithms for which the set of particle radii is strictly fixed, but only below some pressure p_N that vanishes as $N \rightarrow \infty$, above which our predictions should apply.

Hard spheres under swap: The reasoning is identical to soft spheres, except that for hard spheres (i) the pressure \tilde{p} diverges as jamming is approached, and the stiffness of particle interactions diverges as $k \sim \tilde{p}^2$ [17] (ii) marginal stability for non-swap dynamics corresponds to $\delta z \sim \tilde{p}^{-(2+2\theta)/(6+2\theta)}$ where $\theta \approx 0.41$ [24]. Equating the interaction stiffness with k_R leads to a characteristic pressure $\tilde{p}_s \sim 1/\alpha$ beyond which swap starts to affect structure. For larger pressure stability implies $\delta z \geq \alpha^{(2+2\theta)/(6+2\theta)}$, again indicating that isostaticity is lost with swap.

Numerical Model: As shown in Eq. (3), swap dynamics is equivalent to a system of interacting particles which can individually deform. To test our predictions, we consider particles interacting with a half-sided spring

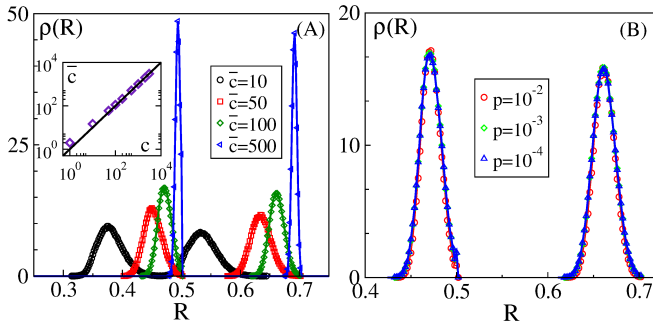


FIG. 2: (A) Distribution of radii $\rho(R)$ for different \bar{c} at fixed $p = 10^{-4}$ and for different p at fixed $\bar{c} = 100$ (B). Inset: $c = k_R/p$ vs $\bar{c} = \bar{k}_R/P$ compared to a linear relation in black. Data are averaged over 1000 systems with $N = 484$ particles. For $\bar{c} = 100$, the width of the distributions are given by $\alpha_1 = 0.0114$ and $\alpha_2 = 0.0124$ for the smaller and bigger radii respectively.

potential:

$$\mathcal{U}(\{r\}, \{R\}) = \frac{1}{2} \sum_{ij} (r_{ij} - (R_i + R_j))^2 \Theta(R_i + R_j - r_{ij}), \quad (9)$$

where $r_{ij} = \|\vec{r}_i - \vec{r}_j\|$. Their radius follow the internal potential:

$$\mu(\{R\}) = \frac{\bar{k}_R}{2} \sum_i (R_i - R_i^{(0)})^2 \left(\frac{R_i^{(0)}}{R_i} \right)^2, \quad (10)$$

where \bar{k}_R is a characteristic stiffness. We considered a potential diverging as $R_i \rightarrow 0$ to avoid particles shrinking to zero size. To avoid crystallisation we further considered that particles are of two types: for 50% of them, $R_i^{(0)} = 1$ while for the others $R_i^{(0)} = 1.4$. This choice leads to a bimodal distribution of size $\rho(R)$, as shown in Fig. 2. Our model corresponds to a swap dynamics where swap is allowed only between particles of the same type.

To study the jamming transition, we consider a pressure-controlled protocol at zero temperature described in the S.I. The chemical potential of Eq. (10) must evolve with pressure to maintain a fixed polydispersity. As shown in Fig. 2.B, it can be achieved within great accuracy simply by imposing that $\bar{k}_R = p\bar{c}$, where \bar{c} is a parameter. (It is inversely proportional to the width α_1 and α_2 of each peak in $\rho(R)$, which play the role of α in the theory above and scale identically as jamming is approached). For our model, the average stiffness $k_R \equiv \langle \partial^2 \mu / \partial^2 R \rangle_i$ is approximatively \bar{k}_R , as shown in the inset of Fig. 2 representing $c \equiv k_R/p$ v.s. \bar{c} .

Structure and Stability: Our central prediction is that for swap dynamics materials must display a larger coordination to enforce stability, as sketched in Fig. 1.B. This prediction is verified in Fig. 3.A, which shows δz v.s. p for various values of \bar{c} . Isostaticity is indeed lost and the coordination converges to a plateau as p decreases. Strikingly, we find for the plateau value $\delta z \sim 1/\sqrt{c} \sim \sqrt{\alpha}$,

consistent with a saturation of the stability bound of Eq. (8). This scaling behavior is implied by the scaling collapse in Fig. 3.B which also confirms that the characteristic pressure below which swaps affects the dynamics scale as $p \sim 1/c \sim \alpha$. Overall, these results supports that the numerical curves $\delta z(p)$ in Fig. 3.A correspond to the marginal stability lines under swap dynamics, shown for different polydispersity (see more on that below).

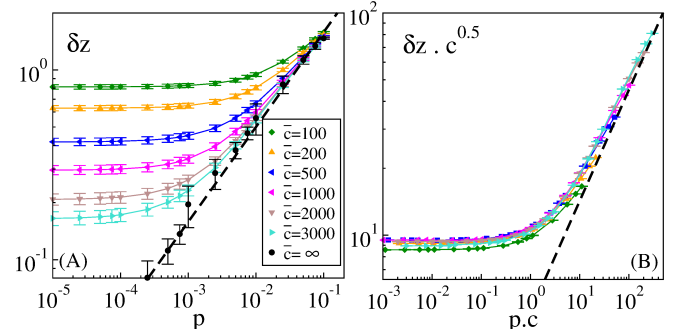


FIG. 3: (A) log-log plot of δz vs. p for different values of \bar{c} as indicated in legend. The black dashed line corresponds to $\delta z \sim \sqrt{p}$. (B) all these curves collapse if the y-axis is rescaled by $c^{0.5}$ and the x-axis is rescaled by c . Bars indicate standard deviations.

Packing fraction: For traditional dynamics, polydispersity tends to have very limited effects on the value of jamming packing fraction ϕ_J . We have confirmed this result in S.I., by showing that although our model can generate very different distributions $\rho(R)$, the values we obtain for ϕ_J cannot be distinguished if jamming is investigated using non-swap dynamics. However, for swap dynamics we expect the situation to change dramatically: since stability requires much more coordinated packings, they presumably need to be denser too. We denote the jamming packing fraction for swap $\phi_c \equiv \lim_{p \rightarrow 0} \phi(p)$. The inset of Fig. 4.A confirms that ϕ_c increases significantly as $\rho(R)$ broadens. To quantify this effect we consider $\phi(p, c)$, as shown in the main panel. Assuming a scaling form for this quantity, and requiring that it satisfies the known results for the jamming transition for $p \gg 1/c$ implies $\phi(p, c) - \phi_J = f(cp)/c^\beta$ where f is some scaling function and $\beta = 1$. Since coordination is not changing for $pc \ll 1$, we expect that it is true for the structure overall and for ϕ , implying that $f(x) \sim x^0$ as $x \rightarrow 0$. These predictions are essentially confirmed in Fig. 4.B. Note however that the best scaling collapse is found for $\beta = 0.83 < 1$. These deviations are likely caused by finite size effects, known to be much stronger for ϕ than for the coordination or vibrational properties [30], and which may thus be present for our system where $N = 484$.

Vibrational properties: We compute the H_{swap} and diagonalize it (see detailed in SI) to extract the density of states $D(\omega)$, as shown in Fig. 5.A for different pressures at fixed polydispersity. As expected, at low p two bands appear in the spectrum. The lowest-frequency band presents a plateau above some frequency scale ω_{swap}^*

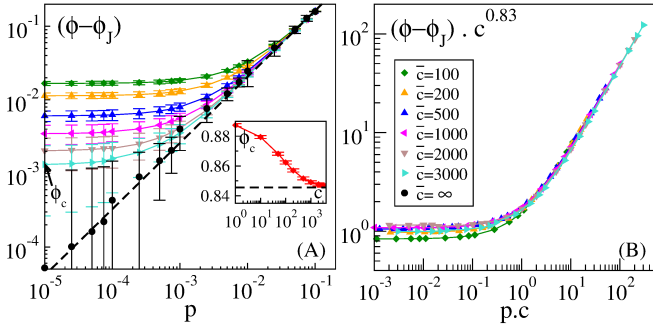


FIG. 4: (A) log-log plot of $\phi - \phi_J$ vs p for different values of \bar{c} . $\phi_J = 0.8456$ is defined as the packing fraction for $c = \infty$ and for the smallest pressure we simulate $p = 10^{-5}$. Inset: ϕ_c vs \bar{c} . ϕ_c is estimated by considering the packing fraction at $p = 10^{-5}$. (B) scaling collapse showing that $\phi(p) - \phi_J \approx f(p)c^{-0.83}$.

which satisfies $\omega_{\text{swap}}^* \sim \sqrt{p}$ as shown in inset, as expected if the structure were marginally stable. As shown in S.I., in the absence of pre-stress the minimal eigenvalues of the Hessian increase many folds, again a signature of marginal stability [19]. Further evidence appears in Fig. 5.B showing $D(\omega)$ at fixed $p = 10^{-4}$ for varying polydispersity. ω_{swap}^* essentially does not depend on \bar{c} as shown in the inset, as expected for marginal packings if the pressure is fixed. The cut-off frequency ω_i of the low-frequency plateau scales as $\omega_i \sim \sqrt{k_R} \sim \sqrt{\bar{c}}$, as predicted above.

These results do support that for swap dynamics, packings lie in the vicinity of an elastic instability as the jamming transition is approached. It is also interesting to consider the softest vibrational modes under swap dynamics far away the jamming transition, as we have argued that these modes are responsible for the fast dynamics observed near the glass transition under swap. We consider in particular $\bar{c} = 1$ and $p = 10^{-2}$ for which $\phi - \phi_J \approx 0.05$, a difference of packing fraction which is of order of the range of ϕ obtained in colloidal glasses. An example of soft modes is shown in Fig. 6, illustrating that the particle displacement is not necessarily divergent free when swap is allowed, since the system can locally compress or expand by changing the particle sizes.

Conclusion: We have shown that in swap algorithms, the dynamics is governed by an effective potential $\mathcal{V}(\{r\}, \{R\})$ that describes both the particles interaction and their ability to deform. As a result, vibrational and elastic properties are softened when swaps are allowed for, while thermodynamic quantities are strictly preserved (when thermal equilibrium is reached). This result first implies that the cross-over temperature T_0 where mechanical stability appears and dynamics becomes activated must be reduced with swap with $T_0^{\text{swap}} < T_0$, leading to a natural explanation as to why the glass transition occurs then at a lower temperature $T_g^{\text{swap}} < T_g$. Our analysis thus supports that near the glass transition, vibrational properties control the nature of elementary

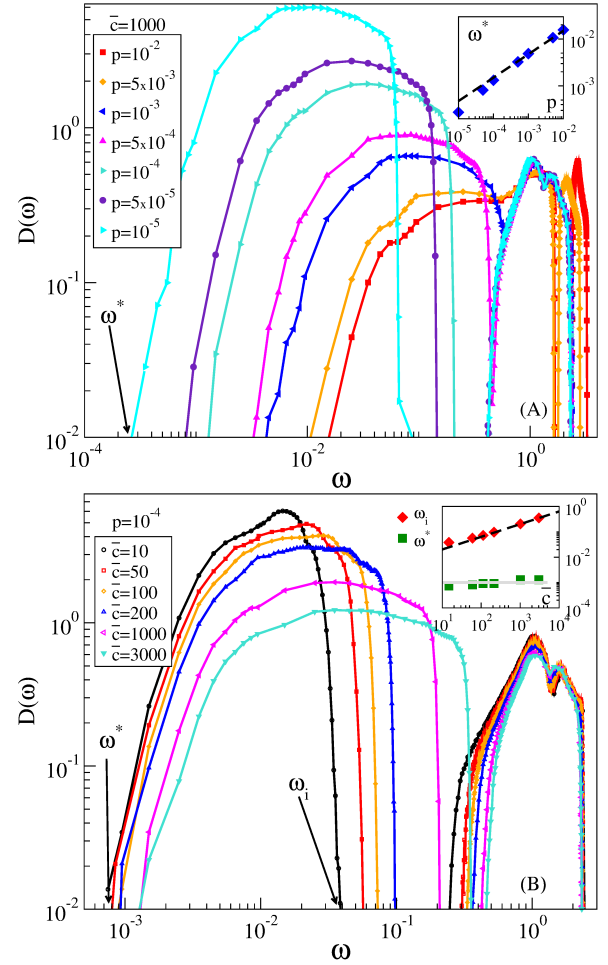


FIG. 5: (A) $D(\omega)$ for different p at fixed $\bar{c} = 1000$. Inset: ω^* vs p , where ω^* is extracted as $D(\omega^*) = 10^{-2}$. Dashed line corresponds to the marginality condition $\omega^* \sim \sqrt{p}$. (B) $D(\omega)$ for different \bar{c} and fixed $p = 10^{-4}$. Inset: ω^* vs p . Dashed line is the theoretical prediction $\omega_i \sim \sqrt{\bar{c}}$ and the continuous line corresponds to $\omega^* = \sqrt{p} = 0.001$.

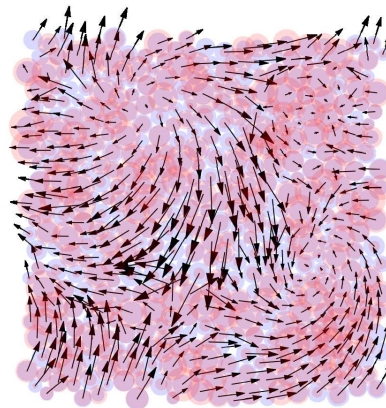


FIG. 6: Example of soft mode with $\omega \approx 0.078$ for $\bar{c} = 1$ and $p = 10^{-2}$. Blue discs indicate the initial particles radii, red discs the new radii induced by motion along that mode. Arrows represent the displacements $\delta \vec{r}_i$ of the particles multiplied by 4 for visualisation.

rearrangements and their associated activation barriers, instead of thermodynamics quantities such as growing static lengths. Secondly, swap must strongly affect the structure of the glass phase. This is particularly striking near the jamming transition that occurs in hard and soft spheres, where we predict that well-known key properties such as isostaticity must disappear. We have confirmed these predictions numerically, and found that for rapid quenches the effective potential $\mathcal{V}(\{r\}, \{R\})$ appears to be marginally stable throughout the glass phase.

Concerning the glass transition, beyond rationalising previous observations of swap algorithms [5–8], our analysis makes additional testable predictions. By increasing continuously the width α of the radii distribution $\rho(R)$, we predict that $T_g^{\text{swap}}(\alpha)$ will smoothly decrease, while $T_g(\alpha)$ should be essentially unchanged. Furthermore, many studies have studied correlations between dynamics and vibrational modes, see e.g. [12, 13, 17, 31], which can be repeated to relate the swap dynamics to the spectrum of the effective potential $\mathcal{V}(\{r\}, \{R\})$. Near T_g , we predict the latter to have more abundant modes at low or negative frequencies than the much studied hessian of the potential energy, and its softest modes to be better predictors of further relaxation processes.

Finally, our work leads to a new method to thermalise liquids by equilibrating directly the potential $\mathcal{V}(\{r\}, \{R\})$, e.g. via Monte-Carlo or molecular dynamics. Our most striking result however is that ultrastable glasses can be built on the computer, simply by *descend-*

ing along the effective potential $\mathcal{V}(\{r\}, \{R\})$. This result appears to contradict theories of the glass transition in which very stable states are reached by growing a static length scale, which requires activation [32]. We predicted and checked that the usual potential energy landscape $\mathcal{U}(\{r\})$ around the obtained configurations does not display excess soft anomalous modes at very low frequency, even near the jamming transition: these modes are gapped. This result explains why marginal stability could not be observed in protocols where a thermal quench was used from swap-generated configurations [33]. Beyond vibrational modes, outstanding questions on the excitations of low-temperature glassy solids could then be probed in these configurations, including the nature of two-level-systems, reported to be almost absent in experimental ultra-stable glasses [34].

Acknowledgments

We thank L. Berthier, G. Biroli, M. Cates, M. Ediger and F. Zamponi for discussions. E. L. acknowledges support from the Netherlands Organisation for Scientific Research (NWO) (Vidi grant no. 680-47-554/3259). M. W. thanks the Swiss National Science Foundation for support under Grant No. 200021-165509 and the Simons Foundation Grant (#454953 Matthieu Wyart).

[1] M. D. Ediger, C. A. Angell, and S. R. Nagel, *J. Phys. Chem.* **100**, 13200 (1996).

[2] C. Angell, *Journal of Non-Crystalline Solids* **131**, 13 (1991).

[3] T. S. Grigera and G. Parisi, *Physical Review E* **63**, 045102 (2001).

[4] L. Fernández, V. Martin-Mayor, and P. Verrocchio, *Physical Review E* **73**, 020501 (2006).

[5] L. Berthier, D. Coslovich, A. Ninarello, and M. Ozawa, *Physical Review Letters* **116**, 238002 (2016).

[6] R. Gutiérrez, S. Karmakar, Y. G. Pollack, and I. Procaccia, *EPL (Europhysics Letters)* **111**, 56009 (2015).

[7] A. Ninarello, L. Berthier, and D. Coslovich, *Phys. Rev. X* **7**, 021039 (2017).

[8] L. Berthier, P. Charbonneau, D. Coslovich, A. Ninarello, M. Ozawa, and S. Yaida, *Proceedings of the National Academy of Sciences* **114**, 11356 (2017).

[9] M. Wyart and M. E. Cates, *Phys. Rev. Lett.* **119**, 195501 (2017).

[10] M. Goldstein, *The Journal of Chemical Physics* **51**, 3728 (1969).

[11] V. Lubchenko and P. G. Wolynes, *Annual Review of Physical Chemistry* **58**, 235 (2007).

[12] K. Broderix, K. K. Bhattacharya, A. Cavagna, A. Zippelius, and I. Giardina, *Phys. Rev. Lett.* **85**, 5360 (2000).

[13] T. S. Grigera, A. Cavagna, I. Giardina, and G. Parisi, *Phys. Rev. Lett.* **88**, 055502 (2002).

[14] J. Kurchan, T. Maimbourg, and F. Zamponi, *Journal of Statistical Mechanics: Theory and Experiment* **2016**, 033210 (2016).

[15] H. Ikeda, F. Zamponi, and A. Ikeda, *The Journal of Chemical Physics* **147**, 234506 (2017).

[16] C. Brito and M. Wyart, *EPL (Europhysics Letters)* **76**, 149 (2006).

[17] C. Brito and M. Wyart, *The Journal of Chemical Physics* **131**, 024504 (2009).

[18] E. DeGiuli, E. Lerner, C. Brito, and M. Wyart, *Proceedings of the National Academy of Sciences* **111**, 17054 (2014).

[19] M. Wyart, L. E. Silbert, S. R. Nagel, and T. A. Witten, *Physical Review E* **72**, 051306 (2005).

[20] P. Charbonneau, J. Kurchan, G. Parisi, P. Urbani, and F. Zamponi, *Nature Communications* **5** (2014).

[21] S. Franz, G. Parisi, P. Urbani, and F. Zamponi, *Proceedings of the National Academy of Sciences* **112**, 14539 (2015).

[22] A. Altieri, S. Franz, and G. Parisi, *Journal of Statistical Mechanics: Theory and Experiment* **2016**, 093301 (2016).

[23] L. Berthier, P. Charbonneau, Y. Jin, G. Parisi, B. Seoane, and F. Zamponi, *Proceedings of the National Academy of Sciences* p. 201607730 (2016).

[24] E. DeGiuli, E. Lerner, and M. Wyart, *The Journal of chemical physics* **142**, 164503 (2015).

[25] S. Alexander, *Physics Reports* **296**, 65 (1998), ISSN 0370-1573.

- [26] M. Wyart, EPL (Europhysics Letters) **89**, 64001 (2010).
- [27] L. Yan, E. DeGiuli, and M. Wyart, EPL (Europhysics Letters) **114**, 26003 (2016).
- [28] E. DeGiuli, A. Laversanne-Finot, G. A. Düring, E. Lerner, and M. Wyart, Soft Matter **10**, 5628 (2014).
- [29] D. Coslovich, L. Berthier, and M. Ozawa, SciPost Physics **3**, 027 (2017).
- [30] C. S. O’Hern, L. E. Silbert, A. J. Liu, and S. R. Nagel, Phys. Rev. E **68**, 011306 (2003).
- [31] A. Widmer-Cooper, H. Perry, P. Harrowell, and D. R. Reichman, Nature Physics **4**, 711 (2008).
- [32] L. Berthier and G. Biroli, Reviews of Modern Physics **83**, 587 (2011).
- [33] C. Scalliet, L. Berthier, and F. Zamponi, arXiv preprint arXiv:1706.04112 (2017).
- [34] D. Queen, X. Liu, J. Karel, T. Metcalf, and F. Hellman, Physical review letters **110**, 135901 (2013).
- [35] S. Franz and A. Montanari, J. Phys. A **40**, F251 (2007).
- [36] G. Biroli and J.-P. Bouchaud, EPL (Europhysics Letters) **67**, 21 (2004).
- [37] E. Bitzek, P. Koskinen, F. Gähler, M. Moseler, and P. Gumbsch, Phys. Rev. Lett. **97**, 170201 (2006).
- [38] H. J. C. Berendsen, J. P. M. Postma, W. F. van Gunsteren, D. A., and H. J. R., Journal of Chemical Physics **81**, 3684 (1984).
- [39] M. P. Allen and D. J. Tildesley, *Computer simulation of liquids* (Oxford university press, 1989).
- [40] This is presumably what MCT seeks to capture [35, 36], but it predicts a length scale that diverges and behaves non-monotonically at the transition. None of these predictions are observed.
- [41] $\rho(R) \equiv \frac{1}{Z} \sum_{\{r\}, \{R\}} \frac{1}{N} [\sum_i \delta(R - R_i)] \exp[-\beta(\mathcal{U}(\{r\}, \{R\}) + \sum_i^N \mu(R_i))].$
- [42] Hybridisation with additional degrees of freedom can only lower the minimal eigenvalues of the Hessian.

Appendix A: SUPPLEMENTAL MATERIAL

This supplemental material (SM) provides: (i) descriptions of the numerical model, protocols and methods used to generate athermal packings under swap dynamics at different pressures, (ii) a computation of the Hessian of the potential energy, together with explanations about how pre-stress affects the vibrational modes, and (iii) a discussion about the effect of the radii distribution generated by swap dynamics on the value of the packing fraction of our athermal packings obtained while freezing the degrees of freedom associated with particles’ radii.

1. Numerical model, protocols and methods

We employ systems of $N = 484$ particles in a square box in two dimensions. The total potential energy depends upon the particles coordinates $\{r\}$ and radii $\{R\}$, as

$$\mathcal{V}(\{r\}, \{R\}) = \mathcal{U}(\{r\}, \{R\}) + \mu(\{R\}). \quad (\text{A1})$$

The pairwise potential term reads

$$\mathcal{U}(\{r\}, \{R\}) = \frac{k}{2} \sum_{ij} (r_{ij} - (R_i + R_j))^2 \Theta(R_i + R_j - r_{ij}), \quad (\text{A2})$$

where k is a stiffness, set to unity, r_{ij} is the distance between the i^{th} and j^{th} particles, and $\Theta(x)$ is the Heaviside step function. The chemical potential associated with the radii is

$$\mu(\{R\}) = \frac{\bar{k}_R}{2} \sum_i (R_i - R_i^{(0)})^2 \left(\frac{R_i^{(0)}}{R_i} \right)^2 \equiv \sum_i \mu(R_i, R_i^{(0)}) \quad (\text{A3})$$

where \bar{k}_R is the stiffness of the potential associated with the radii $\{R\}$, that serves as a parameter in our study, and is set as described below. $R_i^{(0)}$ denotes the intrinsic radius of the i^{th} particle. In each configuration we randomly assigned $R_i^{(0)} = 1$ for half of the particles, and $R_i^{(0)} = 1.4$ for the other half. The mass m of particles, and that associated with their fluctuating radii, are all set to unity. Vibrational frequencies should be understood as expressed in terms of $\sqrt{k/m}$, and pressures in terms of k .

Configurations in mechanical equilibrium at zero temperature and at a desired target pressure p_0 were generated as follows; we start by initializing systems with random particle positions at packing fraction $\phi = 1.2$, and set the initial radii to be $R_i = R_i^{(0)}$. We then minimize the total potential energy $\mathcal{V}(\{r\}, \{R\})$ at a target pressure $p_0 = 10^{-1}$ using a combination of the FIRE algorithm [37] and the Berendsen barostat [38], see futher discussion about the latter below. Each packing is then used as the initial conditions for sequentially generating lower pressure packings, as demonstrated in Fig. 7. Following this protocol, we generated 1000 independent packings at each target pressure, that ranges from $p_0 = 10^{-1}$ up to $p_0 = 10^{-5}$. For each target pressure, we set the stiffness \bar{k}_R of the chemical potential of the radii according to $\bar{k}_R = p_0 \bar{c}$, and vary \bar{c} systematically between 10 and 3000. During minimizations we calculate a characteristic *net* force scale $F_{\text{typ}} \equiv (\sum_i \|\vec{F}_i\|^2 / N)^{1/2}$, where $\vec{F}_i = -\partial \mathcal{V} / \partial \vec{r}_i$ is the net force acting on the i^{th} particle, whose coordinates are denoted by \vec{r}_i . A packing is considered to be in mechanical equilibrium when F_{typ} drops below $10^{-8} p_0$.

Berendsen barostat parameter: The FIRE algorithm [37] features equations of motion which are to be integrated as in conventional MD simulations. We exploit this feature and embed the Berendsen barostat [38] in our Verlet integration scheme [39]. This amounts to scaling the simulation cell volume by a factor χ , calculated as

$$\chi = 1 - \xi \delta t (p_0 - p), \quad (\text{A4})$$

where δt is the (dynamical) integration time step, and ξ is a parameter that determines how quickly the instantaneous pressure converges to the target pressure [39]. In

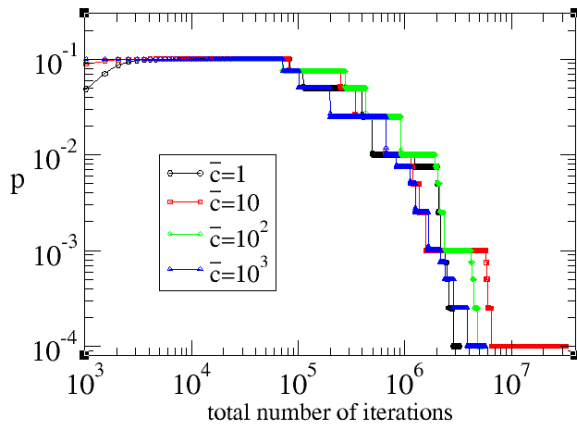


FIG. 7: Pressure p as a function iteration number for a packing-generating simulation starting from one particular initial condition. Each step of the staircase shape of the signal corresponds to the production of a packing at some desired target pressure. The criterion for convergence to mechanical equilibrium at each pressure is explained in the text. We produced packings ranging from $p=10^{-1}$ to $p=10^{-5}$.

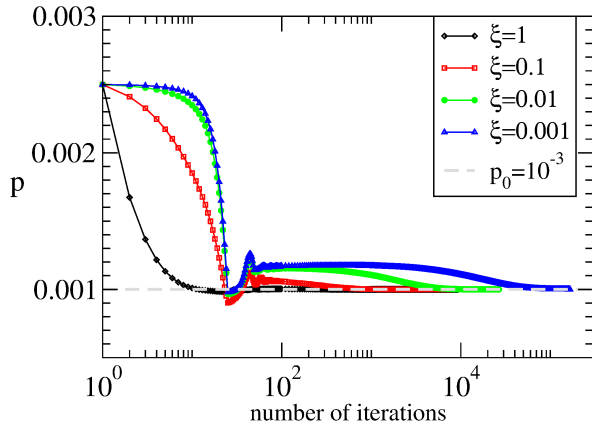


FIG. 8: Instantaneous pressure p as a function of the number of iterations for one initial condition, taken to be $p=0.025$. Here we set $\bar{c}=1000$, fix the target pressure to $p_0=10^{-3}$, and observe the form of the convergence of the instantaneous pressure to the target pressure, for different values of the Berendsen barostat parameter ξ (see definition in text).

Fig. 8 shows the ξ -dependence of the convergence of the instantaneous pressure p to the target value p_0 . Below $\xi = 0.01$, the behavior of p as a function of iteration number is similar. We therefore set $\xi = 0.01$ throughout this work.

2. Computation of H_{swap}

The total potential energy $\mathcal{V}(\{r\}, \{R\})$ of our model system is spelled out in Eqs. (A1)-(A3). We next work out the expansion of \mathcal{V} in term of small displacements $\delta\vec{r}_i$ of particle positions, and small fluctuations δR_i of

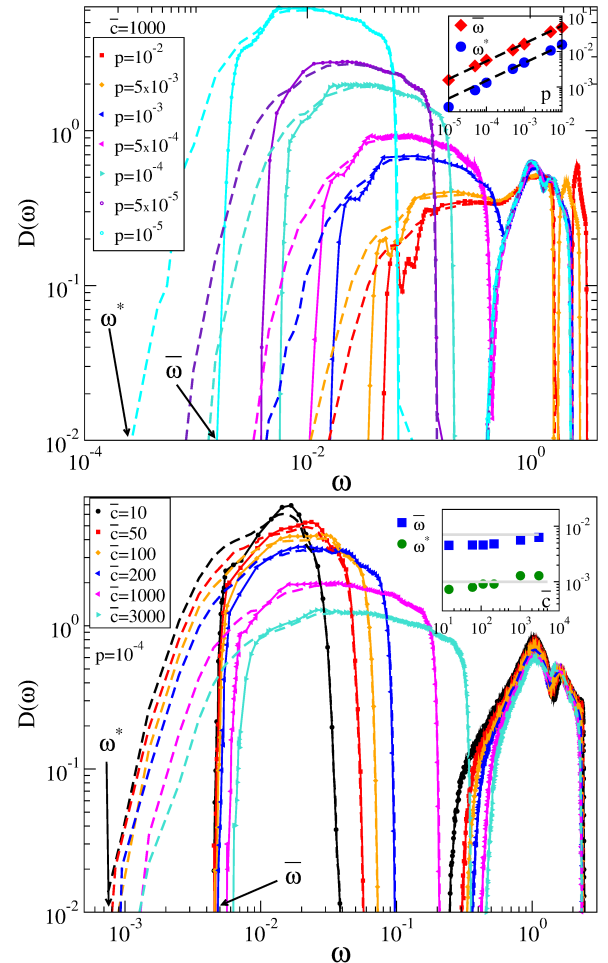


FIG. 9: Top: Density of states $D(\omega)$ for different pressures p at fixed $\bar{c}=1000$, with the pre-stress term included (dashed lines) and excluded (continuous lines). Inset: characteristic frequencies ω^* and $\bar{\omega}$ (as marked in the main panel) vs p . Dashed line correspond to the marginality condition $\omega^* \sim \sqrt{p}$ and $\bar{\omega} \sim \sqrt{p}$. Bottom: $D(\omega)$ for different \bar{c} and fixed $p=10^{-4}$. Note that for these curves $\omega^{*2}/\bar{\omega}^2 \approx 5\%$, indicating that the system is very close to marginal stability.

the radii, about a mechanical equilibrium configuration with energy \mathcal{V}_0 , as

$$\begin{aligned} \delta\mathcal{V} \equiv \mathcal{V} - \mathcal{V}_0 &\simeq \frac{1}{2} \sum_{ij} \delta\vec{r}_i \cdot H_{ij} \cdot \delta\vec{r}_j \\ &+ \frac{1}{2} \sum_{ij} \delta R_i Q_{ij} \delta R_j \\ &+ \sum_{ij} \delta R_i T_{ij} \cdot \delta\vec{r}_j, \end{aligned} \quad (\text{A5})$$

where $H_{ij} \equiv \partial^2 \mathcal{V} / \partial \vec{r}_i \partial \vec{r}_j$, $Q \equiv \partial^2 \mathcal{V} / \partial R_i \partial R_j$, and $T_{ij} \equiv \partial^2 \mathcal{V} / \partial \vec{r}_i \partial R_j$. The expansion given by Eq. (A5) can be written using bra-ket notation as

$$\delta\mathcal{V} = \frac{1}{2} \langle \delta\ell | H_{\text{swap}} | \delta\ell \rangle, \quad (\text{A6})$$

where $|\delta\ell\rangle$ is a $(d+1)N$ -dimensional vector which concatenates the spatial displacements $\delta\vec{r}_i$ and the fluctuations of the radii δR_i : $(\delta\vec{r}_1, \delta\vec{r}_2, \dots, \delta\vec{r}_N, \delta R_1, \dots, \delta R_N)$. The operator H_{swap} can be written as:

$$H_{\text{swap}} = \begin{bmatrix} \begin{bmatrix} H_{N_{d,N_d}} \\ T_{N_{d,N_d}}^T \end{bmatrix} & \begin{bmatrix} T_{N_{d,N}} \\ Q_{N,N} \end{bmatrix} \end{bmatrix}.$$

The elements of the submatrix $H_{N_{d,N_d}}$ can be written as tensors of rank $d=2$ as

$$H_{ij} = \delta_{\langle ij \rangle} \left(\frac{k(r_{ij} - R_i - R_j)}{2r_{ij}} \vec{n}_{ij}^\perp \otimes \vec{n}_{ij}^\perp + \frac{k}{2} \vec{n}_{ij} \otimes \vec{n}_{ij} \right) + \delta_{i,j} \sum_l \left(\frac{k(r_{il} - R_i - R_l)}{2r_{il}} \vec{n}_{il}^\perp \otimes \vec{n}_{il}^\perp + \frac{k}{2} \vec{n}_{il} \otimes \vec{n}_{il} \right),$$

where \vec{n}_{ij} is a unit vector connecting between the i^{th} and j^{th} particles, \vec{n}_{ij}^\perp is a unit vector perpendicular to \vec{n}_{ij} , \otimes is the outer product, $\delta_{\langle ij \rangle} = 1$ when particles i, j are in contact, $\delta_{i,j}$ is the Kronecker delta, and the sum is taken over all particles l in contact with particle i . The elements of the submatrix $Q_{N,N}$ are scalars given by:

$$Q_{ij} = \delta_{\langle ij \rangle} k + \delta_{i,j} \left(\sum_{\langle l \rangle} k + \frac{\partial^2 \mu(R_i, R_i^{(0)})}{\partial R_i^2} \right). \quad (\text{A7})$$

The matrix $T_{N_{d,N_d}}$ is not diagonal and each element can be expressed as a vector with two components given by:

$$T_{ij} = -\delta_{\langle ij \rangle} k \vec{n}_{ij} - \delta_{i,j} \sum_l k \vec{n}_{il}. \quad (\text{A8})$$

The eigenvectors of H_{swap} are the normal modes of the system, and the eigenvalues are the vibrational frequencies squared ω^2 . The distribution of these frequencies is known as the density of states $D(\omega)$.

Effect of the pre-stress on the vibrational modes: When a system of purely repulsive particles is at mechanical equilibrium, forces f_{ij} are exerted between particles in contact. These forces give rise to a term in the expansion of the energy, of the form

$$-\frac{1}{2} \sum_{\langle ij \rangle} \frac{f_{ij}}{r_{ij}} ((\delta\vec{r}_j - \delta\vec{r}_i) \cdot \vec{n}_{ij}^\perp)^2, \quad (\text{A9})$$

often referred to as the “pre-stress term”. For plane waves, it can be shown that the energy contributed by this term is very small. However, for the soft modes present when the system is close to the marginal stability limit, it can be shown that this term reduces the energy of the modes by a quantity proportional to the pressure [19]. Marginal stability corresponds to a buckling transition where the destabilising effect of pre-stress exactly compensates the stabilising effect of being over-constrained. In this scenario where two effects compensate each other,

the eigenvalue of the softest (non-Goldstone) modes of

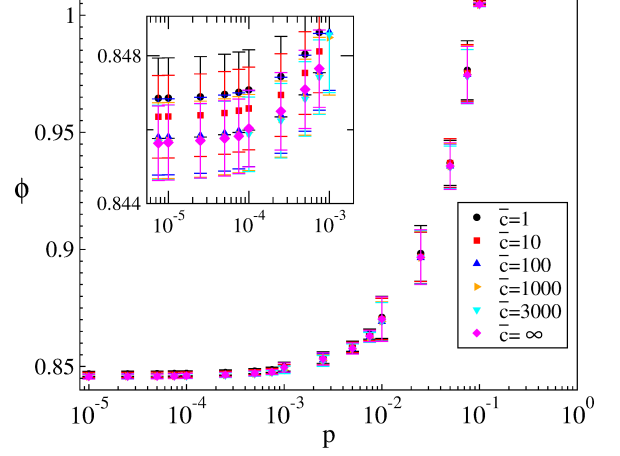


FIG. 10: Packing fraction ϕ as function of pressure p measured for packings in which radii are not allowed to fluctuate, and whose distribution of radii is borrowed from swap packings generated at $p = 10^{-4}$ and at different values of \bar{c} , as indicated by the legend. The inset shows a zoom into very small pressures, demonstrating that the value of ϕ_c depends very weakly on the borrowed distribution of radii of the swap packings, as determined by the parameter \bar{c} .

the Hessian in the absence of pre-stress $\bar{\omega}^2$ must be much larger than ω^{*2} computed when pre-stress is present. To demonstrate this, we have calculated the density of states for systems while including and excluding the pre-stress term. The results are shown in Fig. 9, where it is found that near jamming $\omega^{*2}/\bar{\omega}^2 \approx 5\%$, which is consistent with what previously found for the traditional jamming transition [18] and supports that the system is very close to (but not exactly at) marginal stability.

3. Packing fraction

In the main text we have shown that the jamming packing fraction ϕ_c generated using the swap dynamics increases when $\rho(R)$ broadens, i.e. for smaller values of the parameter \bar{c} that controls the stiffness of the potential energy associated with the radii. Here we compare the dependence of the packing fraction on pressure as measured for systems in which the radii are not allowed to fluctuate. In addition, in this test we borrow the distribution of radii $\rho(R)$ from swap-packings generated at $p = 10^{-4}$, and at various values of the parameter \bar{c} , varied between 1 to ∞ (the latter corresponds to disallowing particle radii fluctuations). Packings were generated using the total potential energy as given by Eq. A2 (with the radii R_i considered to be fixed), and using the same protocol and numerical methods used to generate the swap packings. The results are shown in Fig. 10, where it can be seen that the value of ϕ_c is essentially the same for any borrowed $\rho(R)$ from the swap packings.